A coenergy-based methodology for modeling anisotropy in grain-oriented electrical steel

Abir Janbain, Floran Martin, Guillaume Parent, Olivier Ninet, Anouar Belahcen

A Coenergy-Based Methodology for Modeling Anisotropy in Grain-Oriented Electrical Steel

Abir Janbain[1,2], Floran Martin[2], Guillaume Parent[1], Olivier Ninet[1] and Anouar Belahcen [2] *Senior member, IEEE*

[1]Univ. Artois, UR 4025, Laboratoire Systèmes Electotechniques et Environnement (LSEE), Béthune, F-62400, France
[2] Department of Electrical Engineering and Automation, Aalto University, Espoo, Finland

This work focuses on the vectorization of the magnetic anisotropy model for grain-oriented steel sheets by exploiting coenergy computation and interpolation methods. The proposed approach is based on a modified representation of coenergy isocontours in elliptical form. A novel method for measuring the 2D anhysteretic properties with a rotational single sheet tester is proposed. The model precision is analyzed together with a reduced number of directions.

***Index Terms*—Grain-oriented electrical steel, Magnetic anisotropy, coenergy modeling, elliptical contours, vectorization.**

I. Introduction

GRAIN-ORIENTED electrical steels (GOES) are crucial materials in energy-efficient electrical machines, where magnetic anisotropy is a critical performance factor [1]. This type of steel sheet is manufactured to exhibit a unique crystal structure in which its grains are oriented toward one direction, i.e., the Rolling Direction (RD). Understanding and accurately modeling the anisotropy is important to improve such machine designs and operations [2], [3]. Traditional scalar magnetic models that have been applied so far turned out to be quite effective for applications but lacked the capability of capturing the vectorial behavior of magnetic fields, particularly when energy-based analyses are involved. The coenergy approach creates a promising framework for enhancing the precision and applicability of such models [4]. Advances in computational techniques have further enhanced the applicability of coenergy-based models, enabling their integration into complex CAD tools for electromagnetic design.

For a long time, modeling such anisotropy has been a challenge. The early approaches used diagonal permeability tensors to define the permeability along major directions such as RD, Transverse Direction (TD), and Orthogonal Direction (OD), assuming linear interpolation for the other directions, which proved inaccurate [5]. The nonlinear elliptical models were improvements but still did not capture the full character of the complex anisotropic behavior [6]. The later models based on the first magnetization curves had improved accuracy but required extensive experimental data [7]. The orientation distribution theory models tried to minimize this dependency, but the need for many nonlinear coefficients in those models made them unsuitable for practical engineering use. Recent works, inspired by [8], model the $B(H)$ relationship using Gaussian cumulative distribution functions; this approach has proved promising in balancing accuracy and practicality [9]. However, it considers only the amplitude and hence cannot fully capture the full vectorial behavior of $B(H)$ [10], [11]. This motivates the development of methods that extend these models into a vectorial framework, to fully represent anisotropic magnetic behavior.

Early computational models, such as those based on stored coenergy or energy density functions [12], provided foundational methods to represent anisotropic $B(H)$ curves.

Coenergy-based models have emerged, effectively describing the vectorial $B(H)$ relationship and capturing key features like decoupled magnetization at low fields and the difficult direction at higher fields [4], [13], [14]. By taking advantage of the fact that the relationship $B(H)$ is equivalent to the coenergy density $\omega'(\boldsymbol{H})$, it provides an easy representation of anisotropy, but still physical. The coenergy density $\omega'(\boldsymbol{H})$ represents the volumetric electromagnetic coenergy stored in the material as a scalar function of the applied field H:

$$\omega'(\boldsymbol{H}) = \int_0^{\boldsymbol{H}} \boldsymbol{B}(\boldsymbol{H}) \mathrm{d}\boldsymbol{H}. \tag{1}$$

The $\boldsymbol{B}(\boldsymbol{H})$ relationship is derived directly as the gradient of $\omega'(\boldsymbol{H})$, respecting the energy conservation principles:

$$\boldsymbol{B}(\boldsymbol{H}) = \frac{\partial \omega'}{\partial \boldsymbol{H}}. \tag{2}$$

The coenergy method simplifies the modeling of magnetic anisotropy by reducing the degree of complexity in the representation of the material's behavior. Instead of a vectorial relationship $\boldsymbol{B}(\boldsymbol{H})$, this method uses contours of equal coenergy density $\omega'(\boldsymbol{H})$, naturally encoding the angular dependence of the magnetic response. Such simplification reduces the level of interpolating and parameterizing experimental data.

In this study, the magnetic anisotropy of grain-oriented electrical steel sheets is modeled using a coenergy-based formulation. The magnetic polarization ($\boldsymbol{J} = \boldsymbol{B} - \mu_0 \boldsymbol{H}$) is obtained by magnetic measurement over multiple angular directions. These measurements were performed using a novel 2D spiral demagnetization method under DC bias, enabling the acquisition of the anhysteretic vectorial magnetic characteristics. The stored coenergy is then computed by integrating the scalar product, $\omega' = \int_0^{\boldsymbol{H}} \boldsymbol{J} \cdot \mathrm{d}\boldsymbol{H}$, for each angle. From this dataset, iso-coenergy contours are extracted and plotted in the $(H_x,\ H_y)$ plane. These contours are fitted using a modified elliptical equation, enabling the identification of anisotropy

parameters as functions of energy levels. Finally, the magnetic flux density components B_x, B_y are reconstructed by numerically differentiating the coenergy with respect to H_x and H_y, respectively after adding the vacuum contribution $\mu 0\boldsymbol{H}$. This method provides a fully vectorial description of magnetic anisotropy, surpassing traditional scalar approaches and enabling accurate modeling in arbitrary in-plane directions.

II. Methodology

This work follows a coenergy-based approach supported by experimental 2D anhysteretic measurements. The main steps of the modeling process are described below.

1) 2D Anhysteretic Measurements
   Anhysteretic measurements were performed on grain-oriented electrical steel sheets using a 2D setup. The magnetic field components H_x and H_y, as well as the corresponding magnetic polarization components J_x and J_y, are recorded for various angular directions covering a wide range between the RD and the TD.
2) Computation of Iso-Coenergy Contours
   For each angle, the coenergy ω' is computed from the polarization curves using a trapezoidal numerical integration. From the full set of computed coenergy values, several coenergy levels are selected, uniformly distributed between the lowest and the maximal value of the coenergy. For each coenergy level, the corresponding H_x and H_y values are gathered to form the iso-coenergy contours.
3) Fitting the Modified Elliptical Equation
   The iso-coenergy contours are fitted using a modified elliptical equation of the form:

$$\left(\frac{H_x}{H_{x_0}}\right)^n + \left(\frac{H_y}{H_{y_0}}\right)^n = 1, \tag{3}$$

   where H_{x_0} and H_{y_0} are the intersections of the contour with the RD and TD, respectively. n is an exponent that controls the distortion of the contour and reflects the degree of magnetic anisotropy (Fig. 1). An ellipse is modeled with $n = 2$. It deforms as a rectangle as n approaches infinity. These 3 parameters are interpolated with respect to the coenergy level.

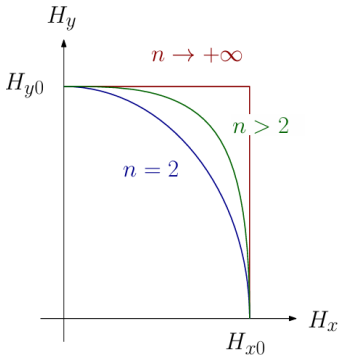

Fig. 1: Evolution of iso-coenergy contours as a function of the shape parameter n.

4) Reconstruction of the Magnetic Flux Density Components
   For a set of (H_x, H_y), the functional parameters $H_{x0}(\omega')$, $H_{y0}(\omega')$, and $n(\omega')$ are unknown. The implicit equation (3) is numerically solved to retrieve the coenergy level corresponding to (H_x, H_y). Then, the coenergy function, $\omega'(H_x, H_y)$, is numerically differentiated with respect to H_x and H_y to compute the magnetic flux density components:

$$B_x = \frac{\partial \omega'}{\partial H_x} + \mu_0 H_x, \qquad B_y = \frac{\partial \omega'}{\partial H_y} + \mu_0 H_y. \tag{4}$$

   This final step allowed the reconstruction of the full vectorial magnetic response based on the coenergy formulation.

A. Experimental Setup and Data Acquisition

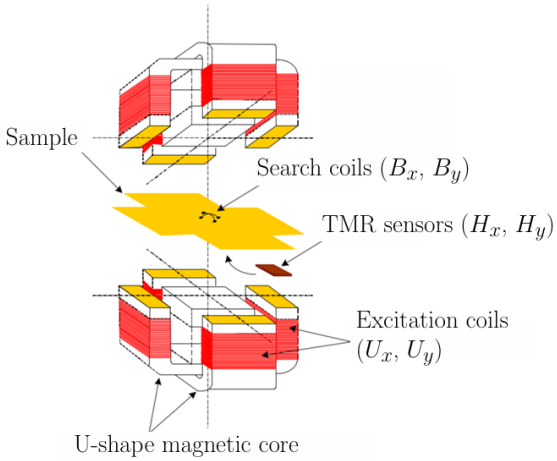

(a) Layout of the 2D Single Sheet Tester (2D SST) showing excitation coils, search coils, and TMR sensors for measuring $\vec{H}$ and $\vec{B}$ in the sample plane.

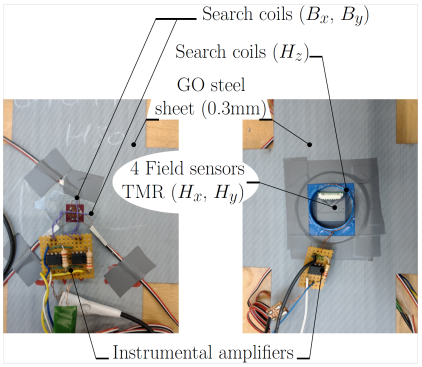

(b) Experimental setup with (0.3mm) grain-oriented (GO) steel sheet, search coils, TMR sensors, and instrumentation for acquiring vectorial magnetic measurements.

Fig. 2: 2D measurement system used to acquire anhysteretic magnetic data: (a) schematic illustration of the 2D SST, and (b) actual implementation with the GO steel sheet and sensors.

To characterize the anisotropic magnetic behavior of (0.3mm) grain-oriented electrical steel, 2D anhysteretic measurements were performed using a customized (2D SST)

capable of controlling both in-plane magnetic field components H_x and H_y, and measuring the corresponding magnetic polarization components J_x and J_y (see Fig. 2).

The anhysteretic response, representing the intrinsic reversible magnetic behavior of the material, was obtained using a spiral demagnetization technique under DC bias conditions (frequency of the demagnetization signal is 50 Hz). This method generates a slowly decaying spiral trajectory in the (H_x, H_y) plane, where the magnitude of the applied magnetic field gradually decreases from the saturation while its direction rotates continuously around the anhysteretic point. As the excitation follows this shrinking spiral path, the magnetization progressively approaches a stable anhysteretic state. The final convergence point, reached when the magnetization ceases to change, is recorded as a representative data point on the anhysteretic surface. This process is repeated for multiple spiral paths

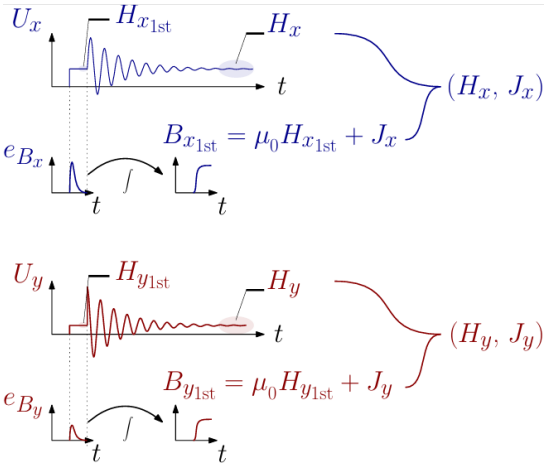

Fig. 3: The excitation coil are supplied with a demagnetizing voltage and a DC bias so that $U_x(t) = U_m \exp -t/\tau \sin(2\pi ft) + U_X$, $U_y(t) = U_m \exp -t/\tau \cos(2\pi ft) + U_Y$. The DC bias ($U_X$, U_Y) is first send to avoid the integration error by the integrator drift. It sends the same flux as the one after the biased demagnetization signal. The TMR sensor is able to measure a DC field, enabling the extraction of the anhysteretic ($\boldsymbol{J}, \boldsymbol{H}$) curve.

oriented in different angular directions relative to the rolling direction (RD), resulting in a dense set of anhysteretic points covering the 2D magnetic space. In this work, measurements are acquired for ten angular orientations: 0°, 10°, 20°, 30°, 40°, 50°, 54.7°, 60°, 70°, 80°, and 90°(see Fig. 4). To ensure directional accuracy during the spiral demagnetization, the DC voltage is precisely controlled to ensure the angular direction of the field within $\mp$ 0.5°. This control is essential to reduce the noise in the measurements.

B. Computation of Coenergy and Iso-Coenergy Contours

To characterize the anisotropic magnetic energy behavior of the material, the stored magnetic coenergy ω' was computed for all the measured angular directions of the magnetic field $\boldsymbol{H}$.

$$\omega' = \int_{\mathbf{0}}^{\boldsymbol{H}} \boldsymbol{J} \cdot \mathrm{d}\boldsymbol{H} \tag{5}$$

The integration is realized with the trapezoidal rule along the measured magnetization paths (Fig. 5).

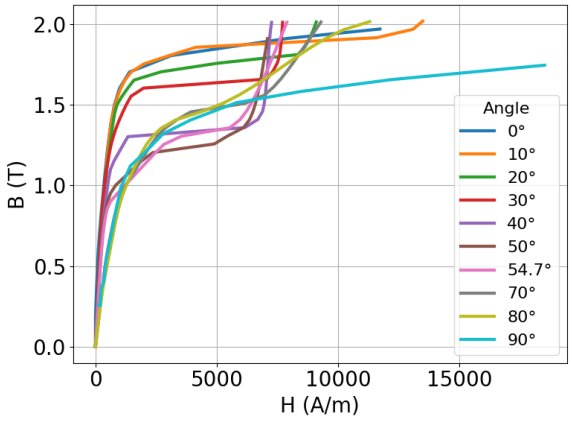

Fig. 4: Experimental $B(H)$ curves measured at ten different angular directions ranging from 0° (RD) to 90° (TD).

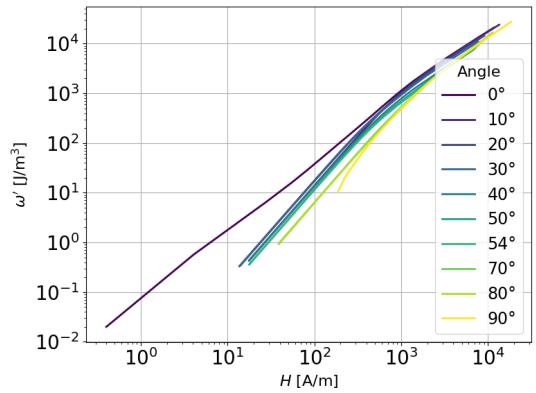

Fig. 5: Stored coenergy curves computed from experimental data at different angular directions.

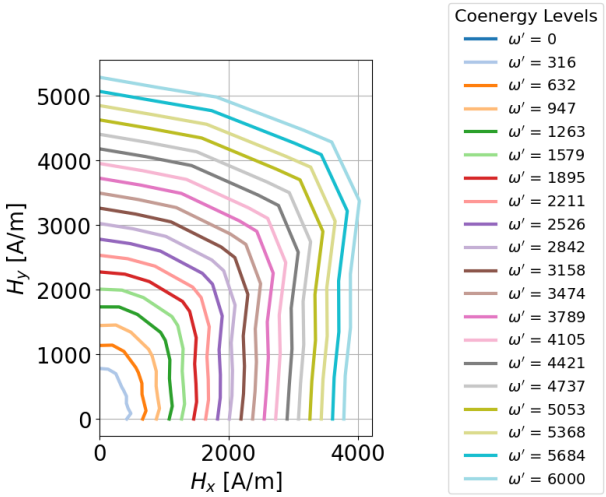

Fig. 6: Extracted iso-coenergy contours in the $H_x - H_y$ plane, used for fitting the anisotropy model.

As expected, the results of the coenergy in the (RD) exhibits the highest magnitude, indicating it is the direction of easiest magnetization. Conversely, the (TD) displays the lowest coenergy, confirming it as the direction of most difficult

magnetization.

To identify the model functional parameters, 20 different contours of coenergy are constructed from the computed 3D curves of coenergy (Fig. 6). The coenergy contours are not overlapping, which confirms a positive-definite behavior, essential for finite element implementation. At higher coenergy levels, the required H_x in the 40° direction becomes slightly higher than in the 0° direction (H_{x_0}). This reflects the increased difficulty of magnetization rotation in intermediate directions, while remaining physically consistent with the anisotropy of the material. Hence, the modified elliptic model should not be able to accurately represent the coenergy near the material saturation. These contours serve as the foundation for identifying the anisotropy through fitting with the modified elliptical equation.

C. Fitting of Iso-Coenergy Contours

The functional parameters $H_{x_0}(\omega')$ and $H_{y_0}(\omega')$ can be easily retrieved without the contours from the measurements along the RD and the TD.

The functional parameter $n(\omega')$ is identified from the coenergy contour by fitting the elliptical equation (3) to the measured one. In order to limit the number of experiments, we propose to investigate the relevant orientations. The contours were fitted using different subset of the experiment:

- Three directions: RD (0°), TD (90°), and one intermediate direction
- Four directions: RD, TD, and any two additional directions,
- Five directions: RD, TD, and three additional directions.

Beyond the numerical error comparison, the geometric evolution of the iso-coenergy contours themselves provides valuable insight. At low coenergy levels, the contours exhibit elliptical shapes, but as the coenergy increases, they gradually becomes closer to a rectangular shape. This implies that the expected values of the shape exponent n should begin close to 2 and increase with coenergy level, but remain finite.

This trend was confirmed during the fitting process using three directions. We systematically tested each angle from 10° to 80° as the third direction, keeping 0° (RD) and 90° (TD) in our dataset. When using either 50° or 54.7° as the third direction, the fitted contours aligned closely with the experimental iso-coenergy contours, and the extracted values of n followed the expected progression: starting near 2 and increasing smoothly. A similar observation was obtained in [4]. Fig. 7b shows the evolution of the fitted values of n across iso-coenergy levels using 50° as third directions. These results (see Fig. 7) are consistent with the physical expectations of anisotropy and demonstrate that a carefully chosen three-direction fitting strategy is sufficient to achieve accurate and reliable parameter identification.

In contrast, using other directions as the third input led to poor fitting performance. In those cases, the values of n showed inconsistent behavior—initially increasing, then decreasing or converging back toward the lower bound of 2. The resulting fitted contours failed to match the deformation observed in the measured data: they started as rectangular, then became

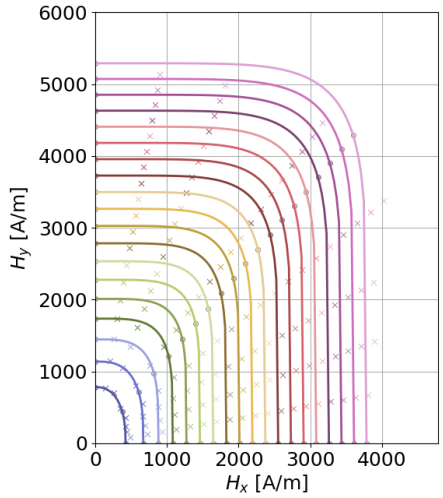

(a) Comparison between iso-coenergy contours and the fitted model using 50° as the third direction. The curves represent the model at each coenergy level and the points (computed coenergy at each angle) marked in × for validation

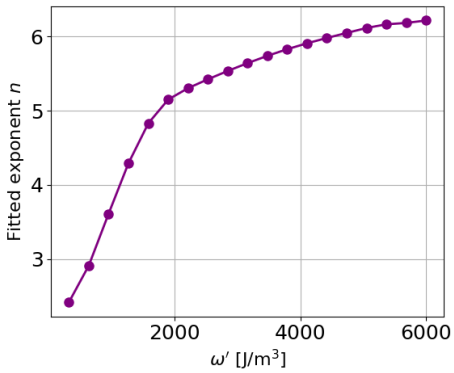

(b) Behavior of the shape exponent n across coenergy levels using 50° as the third direction.

Fig. 7: Example for the fitting performance using 50° as the third direction: (a) the convergence between the model and the iso-coenergy contours, and (b) the evolution of the fitted shape parameter n.

nearly elliptical, indicating a misrepresentation of anisotropy. This mismatch was visually evident in the overlay of the fitted model and experimental contours. In Fig. 8 we will present two graphs, results when using 40° as third direction as an example: one showing the convergence between the experimental iso-coenergy contours and the fitted model, and another showing the evolution of the fitted shape exponent n with respect to the coenergy level. The overlapping contours indicate a non-physical representation of the anisotropy with a non positive definite incremental susceptibility tensor $\partial \boldsymbol{J}/\partial \boldsymbol{H}$.

Moreover, increasing the number of fitting directions to five or seven did not significantly improve the results unless 50° or 54.7° were included. In fact, cases that excluded these angles continued to exhibit fitting deviations and weaker convergence in both the shape of the contours and the final reconstructed magnetic flux density. In Fig. 9 we plotted the evolution curves of the parameter n when using 50° and 54.7° as one of

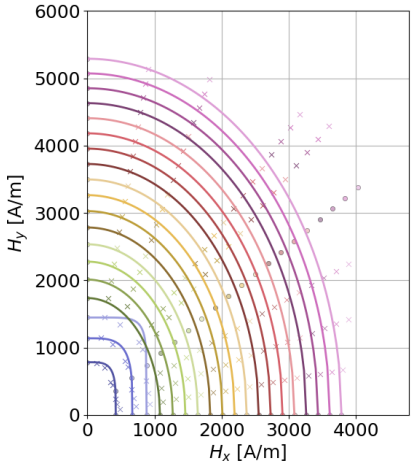

(a) Comparison between iso-coenergy contours and the fitted model using 40° as the third direction.

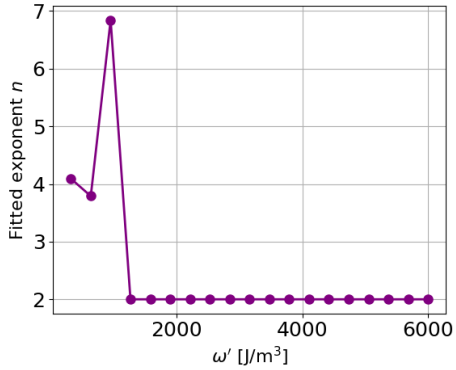

(b) Behavior of the shape exponent n across coenergy levels using 40° as the third direction.

Fig. 8: Example of poor fitting performance using 40° as the third direction: (a) weak convergence between the model and the iso-coenergy contours, and (b) irregular evolution of the fitted shape parameter n.

these directions. The curves show consistent behavior with minimal variation, confirming that three well-chosen directions are sufficient for accurate fitting.

It was observed that using only three directions is sufficient to produce an accurate fit, provided that the third direction is carefully chosen. Among the tested candidates, directions such as 50° and 54.7° provided the lowest error, suggesting they capture the essential curvature of the iso-contours between RD and TD. This justifies our final modeling choice: a three-direction fitting approach using RD, TD, and either 50° or 54.7° as the third angle. It provides a good balance between accuracy and experimental efficiency.

D. Computation and Comparison of B_x and B_y

After validating the use of three well-chosen directions for fitting the iso-coenergy contours, we used the parameters obtained from the modified elliptical equation to numerically compute the magnetic flux density components. This was

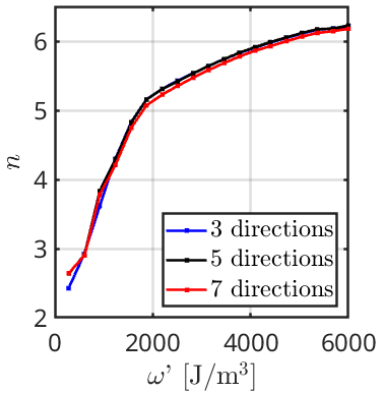

Fig. 9: Evolution of the shape exponent n across iso-coenergy levels using 3, 5, and 7 directions, including either 50° or 54.7° as one of the selected directions.

achieved by differentiating the coenergy function $\omega'(H_x, H_y)$ with respect to H_x and H_y using a central finite difference scheme:

$$J_x = \frac{\partial \omega'}{\partial H_x} \approx \frac{\omega'(H_x + \delta H, H_y) - \omega'(H_x - \delta H, H_y)}{2\delta H},$$
$$J_y = \frac{\partial \omega'}{\partial H_y} \approx \frac{\omega'(H_x, H_y + \delta H) - \omega'(H_x, H_y - \delta H)}{2\delta H} \quad (6)$$

To evaluate the overall fitting accuracy, we computed the Absolute Error (AbsError) between the measured and computed components B_x and B_y for each test angle. Fig. 10 shows the absolute error obtained when using 3 fitting directions. The results when using only three well-chosen directions (including either 50° as a third direction) provide a level of accuracy comparable to using more directions, with minimal error increase.

The flux density components were reconstructed using the coenergy-based expressions (Equation 4). To evaluate the accuracy of the model, we plotted the computed $B_x(H_x)$ and $B_y(H_y)$ curves and compared them with the experimental measurements. Fig. 11 shows this comparison for two representative angles: 70° and 90°.

The results demonstrate good agreement, particularly in the $B_y(H_y)$ curves, where the model accurately reproduces the shape and magnitude of the measured data. The $B_x(H_x)$ component also shows good consistency, though with some deviation in amplitude due to the low field magnitude along that axis at these angles. This is expected, as in directions close to the transverse axis, H_x becomes small, and B_x may exhibit more measurement noise or numerical sensitivity.

Overall, the computed curves reflect the anisotropic behavior well, confirming that the coenergy-based modeling approach, combined with the modified elliptical fitting using three directions, is capable of reliably reconstructing the full vectorial magnetic response of the grain-oriented material.

III. Conclusion

This paper presents a coenergy-based methodology for modeling the magnetic anisotropy of grain-oriented electrical steel.

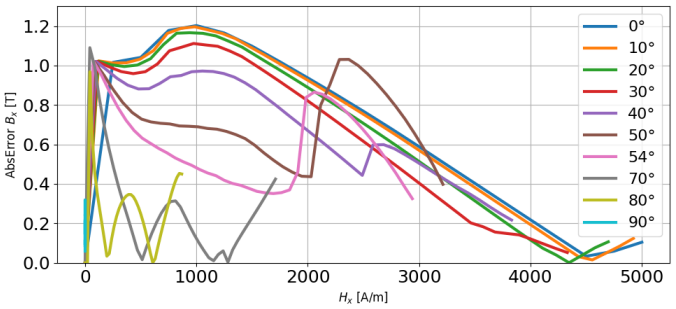

(a) Absolute Error between measured and computed $B_x(H_x)$ at all angles.

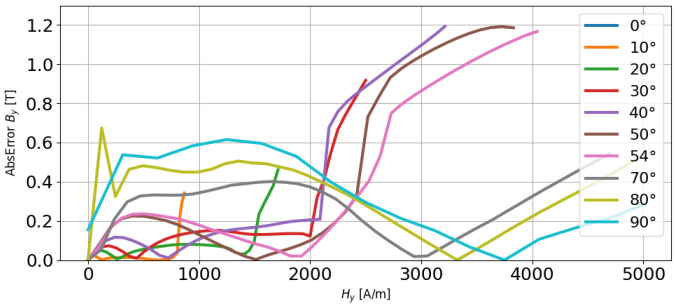

(b) Absolute Error between measured and computed $B_y(H_y)$ at all angles.

Fig. 10: Absolute Error between measured and computed B_x and B_y components for 3 fitting directions and including using 50° as a fitting direction.

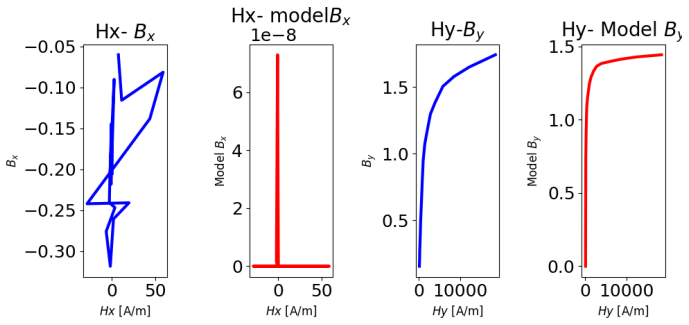

(a) Comparison between measured (blue) and computed (red) magnetic flux density components at 90°.

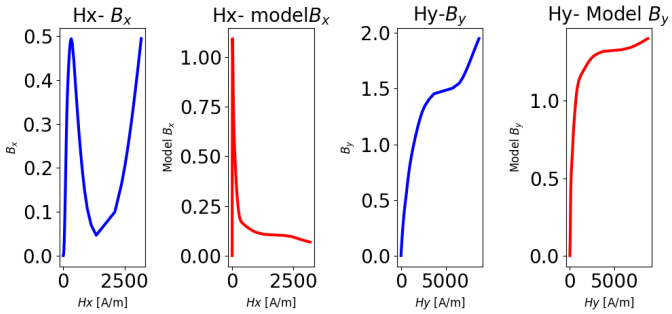

(b) Comparison between measured (blue) and computed (red) magnetic flux density components at 70°

Fig. 11: Curves for magnetic flux density components: measured (blue) and computed (red) at 90° (a) and 70° (b). Each set includes $B_x(H_x)$ and $B_y(H_y)$.

Using a novel 2D anhysteretic measurement procedure, isocoenergy contours are extracted and fitted with a modified elliptical model to capture anisotropic behavior. Although the exctracted isocoenergy contours can not be adequately represented by a modified ellipse when the material approaches the saturation, the reconstructed magnetic flux density presents a good agreement with experimental data, offering a practical and consistent alternative to scalar models. Besides the measurement along the TD and the RD, the hard direction $(54.7°)$ is essential to adequately fit the modified elliptic model. Thanks to the novel 2D anhysteretic measurement method, the characterization along this hard direction is easily accessible.

In the future, we should look after a more accurate model of the coenergy and expand our new measurement methodology to different magnetic materials.

References

[1] J. Maraví-Nieto, Z. Azar, A. S. Thomas, and Z.-Q. Zhu, "Utilisation of grain-oriented electrical steel in permanent magnet fractional-slot modular machines," *J. Eng.*, vol. 2019, no. 17, pp. 3682–3686, Jun. 2019.

[2] F. Jiang, M. Rossi, and G. Parent, "Anisotropy model for modern grain oriented electrical steel based on orientation distribution function," *AIP Adv.*, vol. 8, no. 5, p. 056104, May 2018.

[3] K. Chwastek, M. Najgebauer, J. Szczygłowski, and W. Wilczyński, "Modelling the influence of anisotropy on magnetic properties in grain-oriented steels," *Przeglad Elektrotechniczny*, vol. 87, no. 3, pp. 126–128, Mar. 2011.

[4] T. Péra, F. Ossart, and T. Waeckerle, "Numerical representation for anisotropic materials based on coenergy modeling," *J. Appl. Phys.*, vol. 73, no. 10, pp. 6784–6786, May 1993.

[5] J. ao Pedro Bastos and G. Quichaud, "3d modelling of a non-linear anisotropic lamination," *IEEE Trans. Magn.*, vol. 21, no. 6, pp. 2366–2369, Nov. 1985.

[6] J. M. Dedulle, G. Meunier, A. Foggia, J. C. Sabonnadiere, and D. Shen, "Magnetic fields in nonlinear anisotropic grain-oriented iron-sheet," *IEEE Trans. Magn.*, vol. 26, no. 2, pp. 524–527, Mar. 1990.

[7] K. Chwastek, A. P. S. Baghel, M. F. de Campos, S. V. Kulkarni, and J. Szczyglowski, "A description for the anisotropy of magnetic properties of grain-oriented steels," *IEEE Trans. Magn.*, vol. 51, no. 12, pp. 1–5, Dec. 2015.

[8] D. J. Robertson and D. E. France, "Discrimination of remanence-carrying minerals in mixtures, using isothermal remanent magnetisation acquisition curves," *Phys. Earth Planet. Inter.*, vol. 82, no. 3–4, pp. 223–234, Mar. 1994.

[9] G. C. A. Tolentino, J. V. Leite, M. Rossi, O. Ninet, G. Parent, and J. Blaszkowski, "Modelling of magnetic anisotropy in electrical steel sheet by means of cumulative distribution functions of gaussians," *IEEE Trans. Magn.*, vol. 58, no. 8, pp. 1–5, Aug. 2022.

[10] P. Olszewski, T. Nakata, N. Takahashi, and K. Fujiwara, "Numerical model for soft anisotropic materials and its experimental verification," *J. Magn. Magn. Mater.*, vol. 112, no. 1–3, pp. 447–448, 1992.

[11] F. Ikeda, "2-d magnetic property oriented to magnetic field analysis," *Papers of Joint Technical Meeting on Static Apparatus and Rotating Machinery of IEE Japan*, vol. 4, pp. 33–38, 2004. [Online]. Available: https://cir.nii.ac.jp/crid/1573668924778429696

[12] P. P. Silvester and R. P. Gupta, "Effective computational models for anisotropic soft B-H curves," *IEEE Trans. Magn.*, vol. 27, no. 5, pp. 3804–3807, Sep. 1991.

[13] O. Biro, S. Außerhofer, K. Preis, and Y. Chen, "A modified elliptic model of anisotropy in nonlinear magnetic materials," *COMPEL*, vol. 29, no. 6, pp. 1482–1492, 2010.

[14] F. Martin, D. Singh, A. Belahcen, P. Rasilo, A. Haavisto, and A. Arkkio, "Analytical model for magnetic anisotropy of non-oriented steel sheets," *COMPEL*, vol. 34, no. 5, pp. 1475–1488, Apr. 2015.